Robust Output Feedback Control Design for Inertia Emulation by Wind Turbine Generators

Samaneh Morovati, *Graduate Student Member, IEEE,* Yichen Zhang, *Member, IEEE,* Seddik M. Djouadi, *Senior Member, IEEE,* Kevin Tomsovic, *Fellow, IEEE,* Andrew Wintenberg, *Graduate Student Member, IEEE* and Mohammed Olama, *Senior Member, IEEE*

***Abstract*—Wind generation has gained widespread use as a renewable energy source. Most wind turbines and other renewables connected to the grid through converters result in a reduction in the natural inertial response to grid frequency changes. The doubly-fed induction generator (DFIG) can be controlled to compensate for this reduction and, in fact, provide faster response than traditional synchronous machines. This paper proposes to design observer based output feedback linear quadratic regulator (LQR) and H_∞ control laws to realize the inertia emulation function and deliver fast frequency support. The aim is to track the reference speed by a diesel synchronous generator (DSG) in order to reach the desired inertia. The control signal is computed based on a reduced order model using the balanced truncation technique. A comparison with selective modal analysis (SMA) and balanced truncation model reduction techniques is presented. Comprehensive results show the effective emulation of synthetic inertia by implementing the control laws on a nonlinear three-phase diesel-wind system. The proposed technique is analyzed for different short circuit ratio (SCR) scenarios.**

***Index Terms*—Inertia emulation, diesel-wind system, output feedback control, robust control, balanced truncation model reduction.**

NOMENCLATURE

Mathematical Symbols

Δ	Deviation from operating point
s	Laplace operator
A, B, E	State, control input, disturbance input matrices
C, D, F	Output, control feed-forward, disturbance feed-forward matrices

Physical Variables

All variables are in per unit unless specified.

f_b	Speed base of diesel generator [Hz]
H_D, H_w	Diesel, wind turbine generator inertia constant [s]
H_{rf}	Reference model inertia constant [s]
$i_{dr_{ref}}$	Reference instantaneous rotor current in d-axis
i_{dr}, i_{qr}	Instantaneous rotor current in d, q-axis
i_{ds}, i_{qs}	Instantaneous stator current in d, q-axis
$i_{qr_{ref}}$	Reference instantaneous rotor current in q-axis
K_{P_τ}, K_{I_τ}	Proportional, integral gain of torque controller
K_{P_C}, K_{I_C}	Proportional, integral gain of current controller
K_{P_Q}, K_{I_Q}	Proportional, integral gain of reactive power controller
λ_{dr},λ_{qr}	Rotor flux linkage in d, q-axis
λ_{ds},λ_{qs}	Stator flux linkage in d, q-axis
L_m	Mutual inductance
ω_c	Cut-off frequency of low-pass filter [Hz]
ω_d, ω_r	Diesel, wind turbine angular speed
ω_b	Speed base of wind turbine generator [rad/s]
$\omega_{f_{ref}}$	Filtered reference speed for wind turbine generator
ω_s	Synchronous angular speed
P_g, Q_g	Active, reactive power of wind turbine generators
P_m	Mechanical power of diesel generators
P_v	Valve position of diesel generators
$Q_{g_{ref}}$	Reference reactive power of wind turbine generators
R_D	Governor droop setting of diesel generators
R_{rf}, D_{rf}	Governor droop, load-damping coefficient of reference model
R_s, L_s	Stator resistance, leakage inductance
R_r, L_r	Rotor resistance, leakage inductance
Ψ_s	Space vector of stator flux magnitude
σ	Leakage coefficient of induction machines
τ_m, τ_e	Mechanical, electric torque of wind turbine generators
τ_d, τ_{sm}	Diesel engine, governor time constant [s]
τ_{drf},τ_{smrf}	Reference model time constants [s]
u_c	Supplementary input for model reference control
V_{ds}, V_{qs}	Instantaneous stator voltage in d, q-axis
V_{dr}, V_{qr}	Instantaneous rotor voltage in d, q-axis

I. INTRODUCTION

Diesel synchronous generators (DSGs) are a common choice for powering microgrids in remote locations. A renewable source can reduce the operating cost by partially replacing the usage rate of more expensive diesel generators [1]. Different types of renewable energy sources such as wind and solar are connected to the grid using power electronic interfaces that can ensure power injection at the rated grid frequency [2]. The variable nature of renewable power poses challenges for

*This research was sponsored in part by the Engineering Research Center Program of the National Science Foundation and the Department of Energy under NSF Award Number EEC-1041877 and the CURENT Industry Partnership Program, the National Science Foundation under NSF-ECCS-Awards 1711432 and 1509114, and a Joint Directed Research and Development (JDRD) grant.

S. Morovati, S. M. Djouadi and K. Tomsovic are with the Min H. Kao Department of Electrical Engineering and Computer Science, The University of Tennessee, Knoxville, TN 37996 USA (e-mail: smorovat@utk.edu; mdjouadi@utk.edu; tomsovic@utk.edu).

Y. Zhang is with Argonne National Laboratory, Lemont, IL 60439, USA (e-mail:yichen.zhang@anl.gov).

A. Wintenberg is with the Department of Electrical Engineering and Computer Science, University of Michigan, Ann Arbor, MI 48109, USA (e-mail: awintenb@umich.edu).

M. Olama is with Oak Ridge National Laboratory, Oak Ridge, TN 37831 USA (e-mail: olamahussemm@ornl.gov)

frequency control in mixed diesel-renewable microgrids [3]. This variability can result in large frequency fluctuations without proper controls [4]. Furthermore, unacceptable frequency excursions caused by deterioration of inertial response in the presence of large disturbances can adversely impact system reliability [5]. To address the frequency stability challenges, renewable energy sources need to be equipped with innovative frequency control approaches that contribute to frequency regulation operations [6], [7]. Utilizing stored energy as synthetic inertial response, commonly referred to as inertia emulation, is one of the widely used approaches [8]. These controls can be employed either in grid connected mode or in island mode [9].

Although inertia emulation can be equipped for most converter-interfaced distributed energy resources (DERs), wind turbine generators (WTGs) are the most suitable candidate since the stored kinetic energy in the rotating mass can be readily utilized without additional storage. Existing inertia emulation methods generally couple the stored kinetic energy of WTGs to the rate of change of frequency (ROCOF) [10], [11]. The effective inertial response using such methods can be difficult to quantify as the emulated inertia constant is time varying [12], [13]. Therefore, the system performance cannot be guaranteed. The approach in [14] provides droop control for virtual synchronous generators as a specific control structure to estimate and control inertia. However, this approach needs to use the WTG as a voltage source and at the cost of a de-loaded operation. Besides, adequate frequency stability becomes critical with increasing renewable penetration. The main challenge from the control viewpoint is to keep the system frequency within specified bounds in the presence of disturbances.

In [1] and [15], the authors propose a novel inertia emulation controller for current-mode WTGs. The proposed controller employs the model reference control (MRC) paradigm to precisely emulate programmable inertia constant which guarantees performance on the frequency response. As we know, the MRC is more of a control task than a design method. The H_∞-based state feedback control is employed in [1] and [15] to realize the MRC-based inertia emulation. In order to preserve the original states in the model reduction, the SMA-based model reduction method is used. State feedback control is not very practical since state measurements are not always available. The H_∞ control usually leads to larger gains. Although a technical method is proposed in [1] and [15] to limit the size of the gains, the control signal still has a high peak, and the kinetic energy of WTGs is not optimally utilized.

To resolve the aforementioned issues, an output feedback LQR design is proposed in this paper for MRC realization. In this effort, a Luenberger observer is used to design dynamic output feedback LQR control laws. To simplify the control design, the balanced model reduction technique is used and compared with the SMA technique in capturing system characteristics. We verify the proposed method on a modified 33-node microgrid using a detailed full-order three-phase simulation model in Simulink. The proposed technique is analyzed for different SCR scenarios.

The significance of the proposed method in comparison to the other methods is two-fold. First, compared with the common inertia emulation methods for current-mode DERs that lead to time-varying synthetic inertia responses, we propose the MRC framework, which allows us to emulate the inertia precisely and provide guaranteed performance for the frequency response. We verify the proposed method on the modified 33-node microgrid using a detailed full-order three-phase simulation model in Simulink.

Second, since MRC is more of a control task than a design method, we propose the output feedback LQR and H_∞ controls with the Luenberg observer to realize the MRC-based inertia emulation (IE). Compared with [1] and [15] which use state-feedback control design, the technical benefits are:

1) The output feedback design frees us from the SMA-based model reduction, which is necessary for state feedback control design since it keeps the original state information in the reduced-order model, and allows us to use a variety of model reduction techniques.
2) We employ balanced truncation model reduction and show that it provides higher accuracy compared to the SMA-based approach.
3) We employ both LQR and H_∞ methods to design the output feedback control, and perform a thorough comparative study over these two methods as well as to the proportional-integrator based output feedback control.
4) Since state measurements are not available all the time, the output feedback control is more practical and can be readily applied in a practical implementation.

This paper is organized as follows. Section II briefly introduces the primary objective for inertial response. Section III presents the balanced truncation model reduction technique used for the diesel-wind system and a comparison with the SMA model reduction technique. Section IV describes the proposed observer-based LQR and H_∞ controllers based on inertia emulation strategy. Simulation results are presented in section V, followed by the conclusion in section VI.

II. Objective for Inertial Response

After a power disturbance, online synchronous generators will first limit the ROCOF by converting rotating kinetic energy into electric power, which is known as the inertial response. Then, as the rotor speed slows down the turbine-governor system senses speed deviations and acts to adjust the output of the prime movers to stabilize the rotor speed. The governor response is referred to as the primary frequency control [16]. The time scale of both responses are in terms of seconds. Due to the deadband and response time of the turbine-governor, the inertial response is dominant in the beginning period of frequency decline as shown in Fig. 1. The primary frequency response will then increase to regain power balance and stop the frequency decline. This process is governed by the swing equation:

$$2Hs\Delta\omega = \Delta P_m - \Delta P_d \tag{1}$$

where s is the Laplace operator, $2Hs\Delta\omega$ denotes the inertial response, $\Delta\omega$ denotes the primary frequency response and ΔP_d denotes the disturbance. With more renewable energy penetration, fewer synchronous generators will be committed leading to smaller inertia H in the system, and potentially inadequate inertial response. Wind turbines, for example, are effectively decoupled from grid frequency and will not naturally respond to frequency changes. Thus, controls must be designed to limit the ROCOF if grid support is needed. Controlling the power output proportional and opposing the ROCOF is known as inertia emulation. The traditional approach of an inertia emulation strategy for a WTG is illustrated in Fig. 2. In a such strategy, the stored kinetic energy in a WTG will be released in proportion to ROCOF. The speed of the induction motion will decline due to the energy conversion [12]. Considering the conceptual representation of the inertia emulation in Fig. 2 (b), the swing equation is compensated by the power from the WTG:

$$2Hs\Delta\omega = \Delta P_m - \Delta P_d + \underbrace{G_w(s)K_{\text{ie}}s\Delta\omega}_{\Delta P_g} \tag{2}$$

where $G_w(s)$ represents the dynamic response of WTG to generate the inertia emulation power ΔP_g according to the ROCOF $K_{\text{ie}}s\Delta\omega$. As described in [1] and [10], the configuration in Fig. 2 can only produce synthetic inertial response where the equivalent parameters are time varying and may be difficult to tune. This is easy to see if we rearrange (2) as follows:

$$(2H - G_w(s)K_{\text{ie}})s\Delta\omega = \Delta P_m - \Delta P_d \tag{3}$$

This poses challenges for dynamic security assessment, stability analysis and system performance guarantees. See [1] and [12] for details on the derivation of equivalent parameters of frequency response model under emulated inertia.

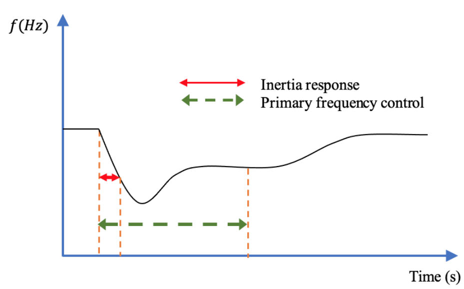

Fig. 1. Typical frequency response after a generator trip.

To overcome the aforementioned difficulties, the objective of our proposed controller is to provide a specific amount of inertia emulation to achieve near-ideal response in the time scale of inertial response in the sense that the equivalent parameters are nearly constant. In other words, we need to compensate the negative effect induced by $G_w(s)$ in (3), which mainly includes the primary mover dynamics and the internal controller response time which is inherent and cannot be compensated by external controllers. So the synthetic inertial response can only be "near-ideal" compared with the conventional inertial response. Fortunately, inner control loops of the converter are too fast (in the time scale of milliseconds) to have sizable impacts on the frequency control [17]. On the other hand, the negative impact induced by the primary mover dynamics, that is, the motion dynamics of the WTG, can be compensated.

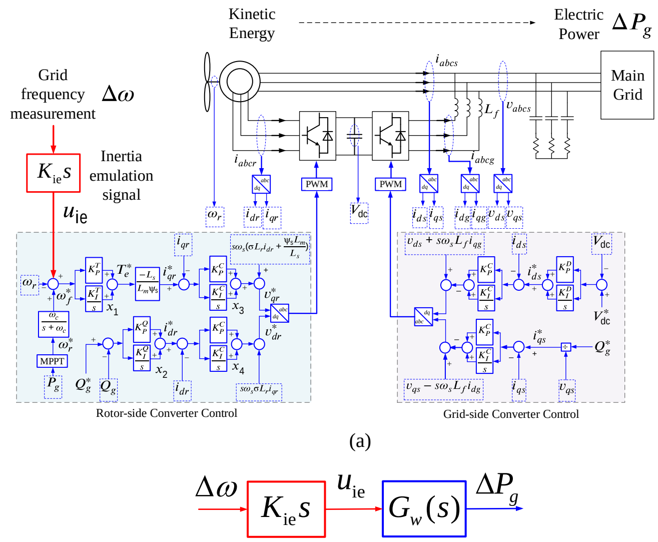

(a)

(b)

Fig. 2. Traditional inertia emulation function within a wind turbine. (a) Detailed view. (b) Conceptual view.

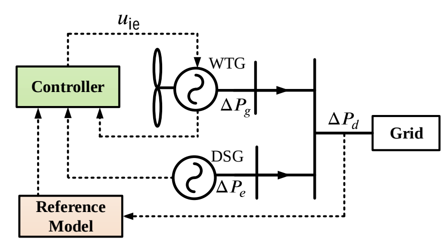

Fig. 3. Model reference control-based inertial emulation control diagram.

The idea to achieve near-ideal synthetic inertial response of WTG can be recast as a tracking problem with respect to a dynamic reference model, known as the MRC. In the MRC, we define a frequency response model with desired parameters as the reference. The objective is to make the DSG speed precisely track the reference frequency using the support from the WTG as shown in Fig. 3. Intuitively, the frequency response of the augmented physical plant consisting of the diesel generator and the WTG will be the same as the response of the reference model. Therefore, the emulated inertia constant is close to the one of the reference model. To see this, let $2H_{rf}s\Delta\omega_{rf}$ and $2H_Ds\Delta\omega_d$ be the inertial response of the reference model and DSG in Fig. 3, respectively, where H_{rf} is the desired inertia constant and $H_{rf} - H_D = H_{\text{ie}} > 0$. The power balance condition holds as:

$$\Delta P_d = 2H_{rf}s\Delta\omega_{rf} = 2H_Ds\Delta\omega_d + \Delta P_g \tag{4}$$

If the speed of DSG can track the speed of the reference model with the support of WTG, that is, $\Delta\omega_{rf} \approx \Delta\omega_d$, then the following relation holds:

$$\Delta P_g \approx 2H_{rf}s\Delta\omega_d - 2H_Ds\Delta\omega_d = 2H_{\text{ie}}s\Delta\omega \tag{5}$$

Therefore, the synthetic inertial response $2H_{\text{ie}}s\Delta\omega_d$ is emulated by the WTG. Traditional strategy in Fig. 2 can be considered as an open-loop control with respect to the WTG since no status information of the WTG is fed back to the inertia emulation module. Since the MRC-based inertia emulation generates the control signal using both grid frequency and WTG states as shown in Fig. 3, it can compensate the negative effect induced by the motion dynamics of WTG. Nevertheless, the MRC is more of a control task than a design methodology. In the following, a mathematical model incorporating both the diesel and WTG will be derived, where an output feedback LQR and H_∞ controllers will be designed to realize the MRC-based inertia emulation.

III. Diesel-Wind System Modeling

In this section, the dynamic model of the WTG is presented. The wind turbine model is assumed to be a type-3 WTG, which is one of the most common wind turbines used in practice. Type-3 wind turbines are also called DFIG-based wind turbines. Note that the proposed paradigm can be applied to any type of converter-interfaced DERs. But WTGs are more readily suitable due to their inherit kinetic energy.

A. Doubly-Fed Induction Generator and Converter Model

The converter of the wind turbine generator includes the rotor-side and grid-side converters, which control the speed of the generator and inject power into the grid, respectively [18]. Since, the rotor-side converter controls the generator speed by regulating the electromagnetic torque, the frequency support function should be included within this subsystem. The grid-side converter has less impact on the frequency support since the time scale of the DC regulation is much faster than the rotor-side control current loop for stability reasons [1].

The differential equations of the fluxes in the dq axes and algebraic equations of the DFIG are given by:

$$\frac{d\lambda_{qs}}{dt} = \omega_b[V_{qs} - R_s i_{qs} - \omega_s \lambda_{ds}] \tag{6}$$

$$\frac{d\lambda_{ds}}{dt} = \omega_b[V_{ds} - R_s i_{ds} + \omega_s \lambda_{qs}] \tag{7}$$

$$\frac{d\lambda_{qr}}{dt} = \omega_b[V_{qr} - R_r i_{qr} - (\omega_s - \omega_r)\lambda_{dr}] \tag{8}$$

$$\frac{d\lambda_{dr}}{dt} = \omega_b[V_{dr} - R_r i_{dr} + (\omega_s - \omega_r)\lambda_{qr}] \tag{9}$$

$$\lambda_{qs} = L_s i_{qs} + L_m i_{qr} \tag{10}$$

$$\lambda_{ds} = L_s i_{ds} + L_m i_{dr} \tag{11}$$

$$\lambda_{qr} = L_r i_{qr} + L_m i_{qs} \tag{12}$$

$$\lambda_{dr} = L_r i_{dr} + L_m i_{ds} \tag{13}$$

The dynamics of the induction machine are presented in (14)-(19), where, τ_m and τ_e are the mechanical and electromagnetic torques ($\tau_e = (L_m/L_s)(\lambda_{qs} i_{dr} - \lambda_{ds} i_{qr})$). $\omega_{f_{ref}}$ is the filtered reference speed for the wind turbine generator and $\omega_{r_{ref}}$ is the reference rotor speed which is computed as an optimal speed based on the maximum power point tracking (MPPT) curve in a relation with the measured electric power as shown in Fig. 4 (Eq. (20)) [19]. The state variables related to the speed controller of the WTG are represented as x_1 and x_2. Also, x_3 and x_4 are defined as state variables related to the reactive power controller. Q_g and P_g are the reactive and active power of the wind turbine generator [20].

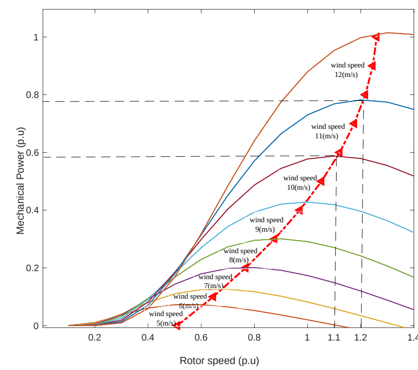

Fig. 4. Mechanical power extracted from wind turbine based on rotor speed.

$$\frac{d\omega_r}{dt} = \frac{(\tau_m - \tau_e)}{2H_w} \tag{14}$$

$$\frac{d\omega_{f_{ref}}}{dt} = \omega_c(\omega_{r_{ref}} - \omega_{f_{ref}}) \tag{15}$$

$$\frac{dx_1}{dt} = K_{I_\tau}(\omega_{f_{ref}} - \omega_r + u_c) \tag{16}$$

$$\frac{dx_2}{dt} = K_{I_Q}(Q_{ref} - Q_g) \tag{17}$$

$$\frac{dx_3}{dt} = K_{I_c}(i_{qr_{ref}} - i_{qr}) \tag{18}$$

$$\frac{dx_4}{dt} = K_{I_c}(i_{dr_{ref}} - i_{dr}) \tag{19}$$

$$\omega_{r_{ref}} = -0.67(P_g)^2 + 1.42(P_g) + 0.51 \tag{20}$$

The algebraic relations of the electric power are expressed in (21) and (22). The loop of algebraic equations is closed by the algebraic relations in (23) and (24) [1], where $\sigma = (L_r L_s - L_m^2)/(L_r L_s)$ is the leakage coefficient of the induction machine.

$$P_g = V_{qs} i_{qs} + V_{ds} i_{ds} + V_{qr} i_{qr} + V_{dr} i_{dr} \tag{21}$$

$$Q_g = V_{qs} i_{ds} - V_{ds} i_{qs} + V_{qr} i_{dr} - V_{dr} i_{qr} \tag{22}$$

$$V_{qr} = x_3 + K_{P_c}(i_{qr_{ref}} - i_{qr}) + (\omega_s - \omega_r)(\sigma L_r i_{dr} + (\frac{\Psi_s L_m}{L_s})) \tag{23}$$

$$V_{dr} = x_4 + K_{P_c}(i_{dr_{ref}} - i_{dr}) - (\omega_s - \omega_r)(\sigma L_r i_{qr}) \tag{24}$$

where $i_{qr_{ref}}$ and $i_{dr_{ref}}$ are expressed by (25) and (26).

$$i_{qr_{ref}} = \frac{-L_s \tau_{e_{ref}}}{L_m \Psi_s} \tag{25}$$

$$i_{dr_{ref}} = x_2 + K_{P_Q}(Q_{g_{ref}} - Q_g) \tag{26}$$

The model used for the DSG is the complete model as described in (27)-(29). This model shows speed changes of the diesel generator based on power, mechanical power and valve position variations [13], [16].

$$\frac{d\Delta\omega_d}{dt} = \frac{f_b}{2H_D}(\Delta P_m - (\Delta P_d - \Delta P_g)) \tag{27}$$

$$\frac{d\Delta P_m}{dt} = \frac{1}{\tau_d}(-\Delta P_m + \Delta P_v) \tag{28}$$

$$\frac{d\Delta P_v}{dt} = \frac{1}{\tau_{sm}}(-\Delta P_v - (\frac{\Delta\omega_d}{f_{base} R_D})) \tag{29}$$

Here, ΔP_d is the disturbance which is the measured power flow variation at a specified location [1] as shown in Fig. 3.

B. Model Reduction Technique

Model reduction is critical for control design of large-scale systems, such as the power grid, as they are governed by differential equations where the number of states can be extremely large [21]. The goal is to provide a low-dimensional model that has a similar response characteristics as the original system and allows a level of storage and computational requirements manageable for practical design and implementation [22].

The model reduction is also beneficial for implementation and deployment of dynamic feedback controllers which are dynamic systems and have the same order as the plant. The full-order plant contains faster electromagnetic dynamics and slower electromechanical dynamics. The former is less relevant to the frequency response, while the latter dominates the frequency behavior. Without model reduction, the controller dynamics will also contain the fast electromagnetic modes that are less relevant to the frequency response but require small steps to simulate, and consume considerable computation resources of the embedded system once deployed.

One popular model reduction technique is the balanced truncation, which is a simple efficient model reduction technique broadly used in reducing model orders of high order linear systems [23]. Balanced reduction was first introduced by Moore [23]. It has been shown to provide accurate reduced order model representations of state-space systems. Since the reduction procedure is based only on system inputs and outputs, model reduction may be heavily dependent on the scaling of the states. However, balanced truncation is independent of the particular system scaling since it uses balanced state space realizations [24].

This paper proposes the balanced reduction method for large scale power systems instead of the traditional reduction method defined as SMA [1]. Although the SMA method has a nice physical interpretation in many cases, it is not the ideal method from a control point of view, since it only relies on certain modes to reduce the order of a large model. We are suggesting a more accurate method that can maintain the main dynamical features of the whole system in the reduced model. The characteristic of this method can help us provide a reliable reduced order model and design a proper, optimized and robust controller to guarantee desired performance.

Assume a stable linear time-invariant system as illustrated by the n dimensional state-space model in (30).

$$\dot{x}(t) = Ax(t) + Bu(t);\ y(t) = Cx(t) \tag{30}$$

In balanced truncation, a balanced realization is first obtained to make the controllability and observability Gramians Q_c and Q_o equal to the diagonal matrix of the Hankel singular values, i.e., $\Sigma = diag(\sigma_1, \ldots, \sigma_N)$. These two Gramians should satisfy the Lyapunov equations:

$$\begin{aligned} &AQ_c + Q_cA^T + BB^T = 0 \\ &A^TQ_o + Q_oA + C^TC = 0 \end{aligned} \tag{31}$$

In addition, Q_c and Q_o form the bases for the controllable and observable subspaces [25]. Hence, the system is balanced when the controllability and observability Gramians are equal [26].

The controllability and observability Gramians are described as follows [26]:

$$Q_o = \int_0^\infty e^{A^Tt}C^TCe^{At}dt;\ Q_c = \int_0^\infty e^{At}BB^Te^{A^Tt}dt \tag{32}$$

In order to transform a realization into a balanced form, a coordinate transformation matrix T is needed to transform the balanced state vector x_b to the original state vector x, where, $x = Tx_b$, such that the transformed observability and controllability Gramians are diagonal and equal [24] as computed by the following equations:

$$\tilde{Q}_o = T^{-T}Q_oT^{-1};\ \tilde{Q}_c = TQ_cT^T \tag{33}$$

The transformation T can be computed by first calculating the matrix $Q_{co} = Q_cQ_o$ [25] and determining its eigenmodes $Q_{co} = T\Sigma^2T^{-1}$. Note that the transformation T is chosen such that the following identities are satisfied [26]:

$$\tilde{Q}_c = \tilde{Q}_o = T^{-1}Q_cT^{-T} = T^TQ_oT := \Sigma \tag{34}$$

So, the balanced state-space model (30) is obtained by taking $TA_bT^{-1} = A$, $C_bT^{-1} = C$ and $TB_b = B$ [26]:

$$\dot{x}_b(t) = A_bx_b(t) + B_bu(t); \quad y_b(t) = C_bx_b(t) \tag{35}$$

The balanced realization gives us the new order of states based on observability and controllability, where the first states are the most controllable and observable states [25]. Hence, (36) expresses the reduced order model by keeping n_r states $(x_1, \ldots, x_{n_r})$ that are the most controllable and observable states and most relevant from the control viewpoint [24].

$$\begin{aligned} &\dot{x}_r(t) = A_rx_r(t) + B_ru(t) \\ &y_r(t) = C_rx_r(t) \end{aligned} \tag{36}$$

Therefore, we can compute the reduced state space matrices using $T_r = \begin{bmatrix} I_r & 0 \end{bmatrix} T$ as:

$$\begin{aligned} &A_r := \begin{bmatrix} I_r & 0 \end{bmatrix} T^{-1}AT \begin{bmatrix} I_r \\ 0 \end{bmatrix}; B_r := \begin{bmatrix} I_r & 0 \end{bmatrix} T^{-1}B \\ &C_r := CT \begin{bmatrix} I_r \\ 0 \end{bmatrix} \end{aligned} \tag{37}$$

The error bound of balanced truncation is given by [26]:

$$\left\|y(t) - y_r(t)\right\|_2 \le 2\sum_{n_r+1}^{n} \sigma_i \left\|u(t)\right\|_2;\ \forall u \in L^2 \tag{38}$$

where L^2 denotes the space of finite energy signals (i.e., the measurable square integrable functions). In order to make the controller design procedure simple, a reduced linearized model about the equilibrium point for the type-3 WTG based on balanced reduction technique is used. A comparison with the SMA technique proposed in [1] is presented. It provides us with a benchmark on how close the reduced model is to the full order linearized model and its performance for all frequency ranges. The linearized full order model of the WTG around the equilibrium point is given as:

$$\Delta\dot{x}_f = A_f\Delta x_f + B_fu_c;\ \ \Delta y_f = C_f\Delta x_f + D_fu_c \tag{39}$$

where

$$x_f = \left[\lambda_{qs}, \lambda_{ds}, \lambda_{qr}, \lambda_{dr}, \omega_r, \omega_{f_{ref}}, x_1, x_2, x_3, x_4\right]^T \tag{40}$$

The full order model is a 10^{th} order model and Δ gives the variation of each variable around the equilibrium. Δy_f is considered as the WTG power output variation, (P_g), due to the inertia emulation input. Then, the reduced order model of the WTG is expressed in (41), where we keep only the most controllable and observable states with the highest Hankel singular value magnitudes and truncate the rest of the state variables from the reduced realization. In other words, we are eliminating the states that are at the same time difficult to control and difficult to observe [22].

$$\begin{aligned}\Delta\dot{x}_{red}(t) &= A_{red}\Delta x_{red} + B_{red}u_c \\ \Delta y_{red} &= C_{red}\Delta x_{red} + D_{red}u_c\end{aligned} \tag{41}$$

where, A_{red}, B_{red}, C_{red} and D_{red} are the state, control input, output and control feed-forward matrices of the reduced order model, respectively.

IV. Control Design

In this section, two different control methods, a LQR and a static state feedback H_∞ control for reference tracking are proposed. Since not all the state variables are available for measurements and only the reduced model is used in the control design stage, a Luenberger observer to estimate the state variables based on the measurements is employed. This results in dynamic output feedback LQR and H_∞ controllers.

A. Linear Quadratic Regulator

A tracking problem is considered for a defined physical plant as an aggregated model of the DSG and WTG. This physical plant is the combination of (27)-(29) and (41) which is given by:

$$\dot{x}_p = A_p x_p + B_p u_c + E_p u_d; \; y_p = C_p x_p \tag{42}$$

where, $x_p = \left[\Delta\omega_d, \Delta P_m, \Delta P_v, \Delta x_{r1}, \Delta x_{r2}, \Delta x_{r3}, \Delta x_{r4}\right]^T$, $y_p = \Delta\omega_d$ and u_d is the disturbance that is considered as the measured power flow variation [1] shown in Fig. 3 and the state-space model is

$$A_p = \begin{bmatrix} 0 & \frac{f_b}{2H_D} & 0 & \frac{f_b[C_{red}]}{2H_D} \\ 0 & \frac{-1}{\tau_d} & \frac{1}{\tau_d} & 0_{1\times4} \\ \frac{-1}{f_b\tau_{sm}R_D} & 0 & \frac{-1}{\tau_{sm}} & 0_{1\times4} \\ 0_{4\times1} & 0_{4\times1} & 0_{4\times1} & [A_{red}] \end{bmatrix}; B_p = \begin{bmatrix} \frac{f_b[D_{red}]}{2H_D} \\ 0 \\ 0 \\ [B_{red}] \end{bmatrix}$$

$$E_p = \begin{bmatrix} \frac{-f_b}{2H_D} \\ 0 \\ 0 \\ 0_{4\times1} \end{bmatrix}; C_p = \begin{bmatrix} 1 & 0 & 0 & 0 & 0 & 0 & 0 \end{bmatrix}$$

The reference signal $(\Delta\omega_{drf})$ for tracking is specified from the reference model similar to the DSG model as:

$$\dot{x}_{rf} = A_{rf}x_{rf} + E_{rf}u_{d_{rf}}; \; y_{rf} = C_{rf}x_{rf} \tag{43}$$

where $x_{rf} = \left[\Delta\omega_{drf}, \Delta P_{mrf}, \Delta P_{vrf}\right]^T$, $y_{rf} = \Delta\omega_{drf}$ and

$$A_{rf} = \begin{bmatrix} \frac{-f_b D_{rf}}{2H_{rf}} & \frac{f_b}{2H_{rf}} & 0 \\ 0 & \frac{-1}{\tau_{drf}} & \frac{1}{\tau_{drf}} \\ \frac{-1}{f_b\tau_{smrf}R_{rf}} & 0 & \frac{-1}{\tau_{smrf}} \end{bmatrix}; E_{rf} = \begin{bmatrix} \frac{-f_b}{2H_{rf}} \\ 0 \\ 0 \end{bmatrix}$$

$$C_{rf} = \begin{bmatrix} 1 & 0 & 0 \end{bmatrix}$$

To formulate the control problem, we consider the LQR cost function:

$$J = \int_0^\infty [x^T Q x + u^T R u] dt \tag{44}$$

where $Q = C^T Q' C$ is a diagonal, symmetric, positive semi-definite matrix of $\Delta\omega_d - \Delta\omega_{drf}$ weights and R is a diagonal, symmetric, positive definite matrix of control weights. The optimal control problem minimizes (44) over all controls $u \in L^2(0,\infty)$ with the tracking constraint. The LQR problem has a unique solution for a controllable system and the optimal input u^* is given by [26]:

$$u^* = -Kx = -\left[K_p, K_{rf}\right]x \tag{45}$$

Finally, the augmented closed loop system $x_{aug} = \left[x_p, x_{rf}\right]^T$ is defined below:

$$\begin{aligned}\dot{x}_{aug}(t) &= \hat{A}x_{aug}(t) + \hat{B}x_{aug}(t) + \hat{E}d(t) \\ y(t) &= y_p - y_{rf} = \hat{C}x_{aug}(t) + \hat{D}x_{aug}(t)\end{aligned} \tag{46}$$

where, $d = [u_d, u_{d_{rf}}]$, $\hat{C} = [C_p, -C_{rf}]$, $\hat{D} = [D_pK_p, D_pK_{rf}]$, $\hat{A} = \begin{bmatrix} A_p & 0 \\ 0 & A_{rf} \end{bmatrix}$, $\hat{B} = \begin{bmatrix} B_pK_p & B_pK_{rf} \\ 0 & 0 \end{bmatrix}$ and $\hat{E} = \begin{bmatrix} E_p & 0 \\ 0 & E_{rf} \end{bmatrix}$.

To compute the feedback law, the observer in (47) is used to estimate the states and we use the physical plant output measurements to get an output feedback controller as an inertia emulation controller. Therefore, the LQR based-observer controller is expressed as follows:

$$\begin{aligned}\dot{\hat{x}}(t) &= \hat{A}\hat{x}(t) + \hat{B}u^* + L(y(t) - \hat{y}(t)) + \hat{E}d(t) \\ \hat{y}(t) &= \hat{C}\hat{x}(t)\end{aligned} \tag{47}$$

which can be written as:

$$\begin{aligned}\dot{\hat{x}}(t) &= (\hat{A} + \hat{B}K - L\hat{C})\hat{x}(t) + Ly(t) + \hat{E}d(t) \\ u_{ie} &= K\hat{x}(t)\end{aligned} \tag{48}$$

where L is any matrix such that $\hat{A} - L\hat{C}$ is stable [26].

The LQR feedback law is applied to the nonlinear system and compared to the H_∞ controller in Section V.

B. H_∞ Control

The theoretical formulation of the H_∞ control problem has been addressed in many books and papers, see [26] for example. In this section, we use a static state feedback control for reference tracking based on the H_∞ control structure fully described in [1]. In this case, the objective is the sub-optimal problem:

$$\min \left\|G_{y/d}\right\|_{\infty} < \gamma ; \quad \gamma > 0 \tag{49}$$

where $G_{y/d}$ is the transfer function from the disturbance to the tracking error where $\left\|G_{y/d}\right\|_{\infty}$ is defined as $\sup_{ess} \bar{\sigma}(G_{y/d}(j\omega))$ [26]. $\bar{\sigma}(.)$ is the largest singular value of $G_{y/d}(j\omega)$. Equivalently, we can solve the multi-objective optimization problem defined in (50). Necessary and sufficient conditions for solving this problem are presented in [1]:

$$\begin{aligned} &\min \gamma + \alpha + \beta \\ &\begin{bmatrix} -\alpha I & \bar{K} \\ \bar{K} & -I \end{bmatrix} < 0 \,, \quad \begin{bmatrix} \beta I & I \\ I & -\bar{P} \end{bmatrix} > 0 \,, \quad \bar{F} < 0 \end{aligned} \tag{50}$$

where there exists scalar variables $\gamma, \alpha, \beta > 0$ and matrix variables $\bar{P}, \bar{Q}, \bar{L}_i > 0$, $\bar{M}_i, \bar{V}_i$ for $i = 1, 2$ and $\bar{K}$. $\bar{F}$ is a symmetric linear matrix inequality (LMI), which can be computed based on [1]. Therefore, the controller given in (45) can guarantee the system performance, where the static gain $K = \bar{K}\bar{P}^{-1}$. Hence, similar to the LQR case, the use of the Luenberger observer gives a dynamic controller based on the computed static H_∞ control, and results in a dynamic output feedback controller.

The control structure for the LQR and H_∞ as output feedback control for reference tracking based on inertia emulation control is illustrated in Fig. 5. The controller $\hat{K}$ is a dynamic output feedback controller based on the observer expressed in (48). The signal d represents disturbances and Z represents measurements while y denotes the observed outputs ($\Delta\omega_d$ and $\Delta\omega_{drf}$) from the physical plant. The dynamic of the controller $\hat{K}$ can be represented by

$$\begin{aligned} \dot{\hat{x}}(t) &= (\hat{A} + \hat{B}K - L\hat{C})\hat{x}(t) + Ly(t) \\ u_{ie}(t) &= K\hat{x}(t) \end{aligned} \tag{51}$$

where the controller K is designed based on the LQR or H_∞ control techniques.

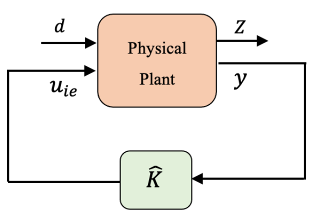

Fig. 5. Output feedback observer-based control.

V. Numerical Results

The proposed controllers are applied to a modified 33-bus microgrid simulated using MATLAB Simulink platform [27], [28]. The closed-loop system performance is tested using the single diesel-wind system described in [1]. The WTG model is modified based on the DFIG in the Simulink demo library by changing the aerodynamic model to the one detailed in [20], where a two-mass model is reduced to the swing equations with combined inertia of the turbine and generator [1].

For simulation purposes, time constants of turbine-governor system in the reference model are considered equal to that in the diesel synchronous generator. Moreover, we only consider tuning the inertia constants of the reference model and do not emulate load damping effects [29]. The system parameters are given in Appendix A.

A. Model Reduction Results

The reduced 4^{th} order model of the WTG is expressed in (53). Since there are only 4 states with the highest Hankel singular value magnitudes, we keep only the 4 most controllable and observable states and truncate the rest of the state variables from the reduced realization. In other words, we are eliminating the states that are at the same time difficult to control and difficult to observe [22]. The Hankel singular values are:

$$\begin{aligned} H_s = [&1.6 \quad 1.2 \quad 1.1 \quad 1.1 \quad 0.02 \quad 0.01 \quad 0.003 \\ &0.0005 \quad 0 \quad 0]^T \end{aligned} \tag{52}$$

Observe the sharp decrease in the magnitudes of the singular values after the 4^{th} one justifying keeping only 4 state variables and eliminating the rest in the following reduced model:

$$\begin{aligned} \Delta\dot{x}_{red}(t) &= A_{red}\Delta x_{red} + B_{red}u_c \\ \Delta y_{red} &= C_{red}\Delta x_{red} + D_{red}u_c \end{aligned} \tag{53}$$

where,

$$A_{red} = \begin{bmatrix} -638.5 & -35.1 & 72.05 & -288.3 \\ 35.1 & -0.06 & 0.13 & -101.1 \\ -72.05 & 0.13 & -0.28 & 353.7 \\ -288.3 & 101.1 & -353.7 & -135.6 \end{bmatrix};$$

$$B_{red} = \begin{bmatrix} -45.87 \\ 0.37 \\ -0.8 \\ -17.25 \end{bmatrix}$$

$$C_{red} = \begin{bmatrix} 45.87 & 0.37 & -0.8 & 17.25 \end{bmatrix}; \; D_{red} = 0.94$$

A comparison of the accuracy using balanced truncation and SMA methods are presented in Fig. 6. As shown, we can capture the full order model precisely. In addition, H_∞ norms for the difference between the reduced model transfer function and the full order transfer function ($\left\|G_{full} - G_{red}\right\|_{\infty}$), where $\left\|.\right\|_{\infty}$ is the H_∞-norm, are given in Table I. Balanced truncation can reduce the order of the model with a much lower H_∞ norm, validating the accuracy.

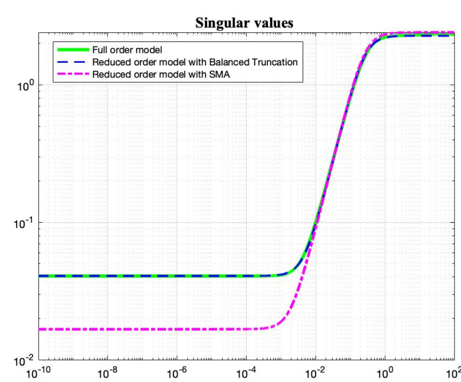

Fig. 6. Singular values of full order model and reduced models.

TABLE I
H_∞ NORMS COMPARISON OF REDUCED ORDERED MODELS

Reduction Method	H_∞ Norm
Balanced Truncation	0.065
SMA	3.707

The responses of the nonlinear system and the reduced order linear model are compared in Fig. 7 in order to validate the latter under a step signal input. As shown in Fig. 7, the modeling error using the balanced truncation is not significant. The mean squared error between the reduced order model and nonlinear model for the speed of the DSG (ω_d), WTG active power variation (P_g) and mechanical power variation of diesel generator (P_m), captured as 0.034Hz, 1.4×10^{-6}W and 0.0013MW, respectively. The closed-loop system performance subject to a step load change at bus 18 as a disturbance is considered for two different cases.

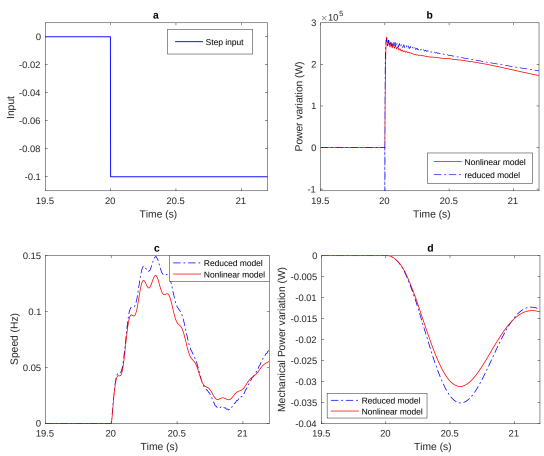

Fig. 7. Response comparison of nonlinear and reduced order model physical plant. (a) Step input. (b) WTG active power variation. (c) Speed of DSG. (d) Mechanical power variation of diesel generator.

B. Case I

For the first case, the desired inertia in the reference model is two seconds, that is, $H_{rf} = 2$, and the inertia constant of the DSG is set to one second, that is, $H_D = 1$. In other words, we will emulate one second inertia constant from the WTG, that is, $H_{\text{ie}} = 1$. Under the MRC paradigm, we compare three design approaches, that is, LQR, H_∞, and a simple proportional–integral (PI) controller. We also compare the MRC paradigm with the conventional inertia emulation method. The ROCOF is obtained by a washout filter $k_i s/1 + 0.01s$. We index the aforementioned controllers as follows:

- Controller 1: MRC-based IE with LRQ realization
- Controller 2: MRC-based IE with H_∞ realization
- Controller 3: MRC-based IE with PI realization
- Controller 4: Conventional IE using a washout filter

The feedback gains obtained for Controllers 1 and 2 are given in (54) and (55):

$$K_{lqr} = [-9.98 \quad -2.27 \quad 0.01 \quad -4.25 \quad 0.04 \quad -0.41 \quad -0.47 \quad 9.94 \quad 1.06 \quad -0.04] \tag{54}$$

$$K_{H_\infty} = [83.01 \quad 2.98 \quad 0.17 \quad 18.74 \quad 0.42 \quad 2.33 \quad 2.24 \quad -83.38 \quad -2.39 \quad 0.12] \tag{55}$$

The PI gain for Controller 3 is obtained via the pidtune function in Matlab and given as $K_p = 0.0113$, $K_I = 0.6471$. The IE gain for Controller 4 can be determined based on Eq. (3), that is, $k_i = -H_{\text{ie}}/(2f_b)$. To emulate one second inertia constant, we set $k_i = -0.03$. The closed-loop performance is illustrated in Fig. 8. As shown, the synthetic inertia constant is accurately emulated using Controllers 1 and 2. However, both Controllers 3 and 4 have tracking errors. Fig. 8 (a) and (b) present the control inputs and the power outputs of the WTG, respectively. Note that there exists a weak inertial response for the field-oriented controlled DFIG-based WTG even without a supportive controller, and this response is sensitive to the rotor current-controller bandwidth and cannot provide the exact synthetic inertia. To have a precise comparison, the tracking error for each realization is shown in Fig. 8 (d). It can be readily observed that Controller 2 outperforms all controllers followed by Controller 1 with the objective to remove tracking error to get precise emulated inertia.

C. Case II

In the second case, setting the desired inertia to five seconds ($H_{rf} = 5$), the closed-loop performance using MRC based IE with different realizations is illustrated in Fig. 9. We use the same indices as in the previous subsection to denote the controllers. In this case the computed feedback laws (56) and (57) for Controller 1 and 2 are

$$K_{lqr} = [-9.98 \quad -2.27 \quad 0.01 \quad -4.25 \quad 0.04 \quad -0.41 \quad -0.47 \quad 9.87 \quad 0.33 \quad -0.05] \tag{56}$$

$$K_{H_\infty} = [288.9 \quad 5.86 \quad 0.20 \quad 44.43 \quad 1.35 \quad -3.51 \quad 13.30 \quad -289.16 \quad -1.21 \quad 0.019] \tag{57}$$

The re-tuned PI gains for Controller 3 are $K_p = 1.29$ $K_I = 4.56$. For conventional IE (Controller 4), based on $k_i = -H_{\text{ie}}/(2f_b)$, to emulate four seconds inertia constant, we set $k_i = -0.12$. The performance of all controllers is shown in Fig. 9. As seen in the figure, small tracking errors are obtained by Controllers 1 and 2, that is, the closed-loop system can emulate the desired inertia under the presence of disturbance. It is clear that if the desired inertia defined by the reference model increases, Controllers 3 and 4 are unable to track the reference frequency well and their tracking errors are higher relative to the LQR and H_∞ controllers. It can also be observed that Controller 2 outperforms all controllers followed by Controller 1. For Cases I and II, the H_∞ controller performs better than the LQR and PI controllers since it has improved robustness properties in the presence of plant uncertainties, that is the discrepancy between the reduced order linear model and the full order nonlinear model.

D. Control Performance for Different Short Circuit Ratios

As known, the SCR is often used as an index for the connection strength. The SCR of a strong grid is discussed in [30], [31], [32]. The SCR is defined as the ratio between short circuit apparent power from a 3-line to ground fault at a given

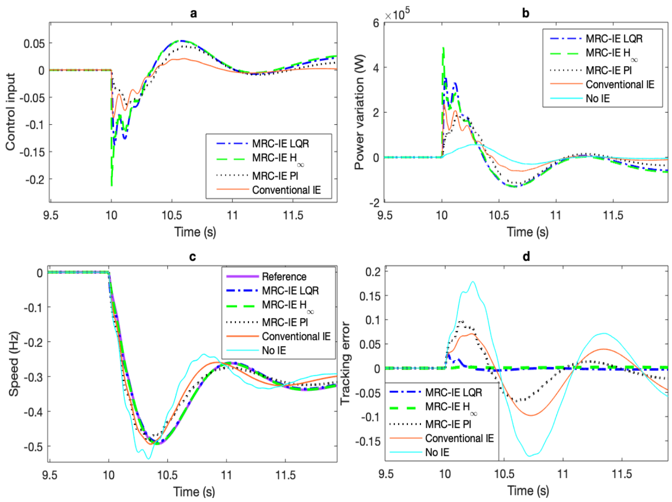

Fig. 8. Closed-loop performance under MRC based IE with LQR, H_∞, PI controllers realization and conventional IE with desired inertia set to two second. (a) Control input. (b) Active power variation of WTG. (c) Speed of DSG. (d) Tracking error.

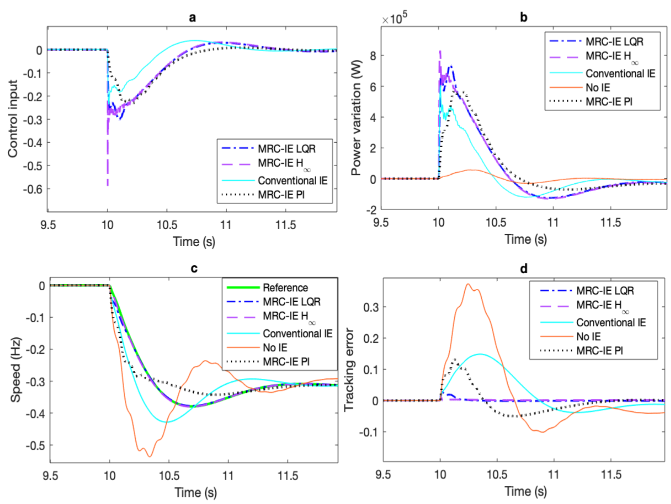

Fig. 9. Closed-loop performance under MRC based IE with LQR, H_∞, PI controllers realization and conventional IE with desired inertia set to five second. (a) Control input. (b) Active power variation of WTG. (c) Speed of DSG. (d) Tracking error.

location in the power system to the rating of the inverter-based resource connected to that location [33]. As the numerator of SCR relies on the specific measurement location, this location is usually stated along with the SCR number that is defined as:

$$\mathrm{SCR} = \frac{\mathrm{MVA_{SC}}}{\mathrm{MW_n}} \tag{58}$$

where $\mathrm{MVA_{SC}}$ is the short circuit MVA level at the point of interconnection (POI) without the current contribution of the WTG, and $\mathrm{MW_n}$ is the nominal power rating of the WTG being connected at the POI. Here to analyze the sensitivity of the proposed technique, the closed-loop system performance for different SCR values is provided by implementing the MRC based inertia emulation with LQR and H_∞ controllers. The SCR values for three different scenarios in a range of (1.95,5) are provided in Table II where the $\mathrm{MW_n} = 1.1$MVA.

TABLE II
SCR VALUE FOR DIFFERENT SCENARIOS

$\mathrm{MVA_{SC}}$	SCR
2.1	1.95
3.4	3.1
5.6	5.1

The performance for the MRC based inertia emulation with LQR and H_∞ controllers, by setting all parameters and controllers similar to Case II, are provided in Fig. 10 and Fig. 11, respectively. As it is clear, both proposed controllers can emulate the desired inertia with a small tracking error. The tracking error varies in a negligible range for all scenarios. The captured SCR lower bound by simulations is 0.26, that is the system performance with the proposed techniques is guaranteed for SCR ≥ 0.26.

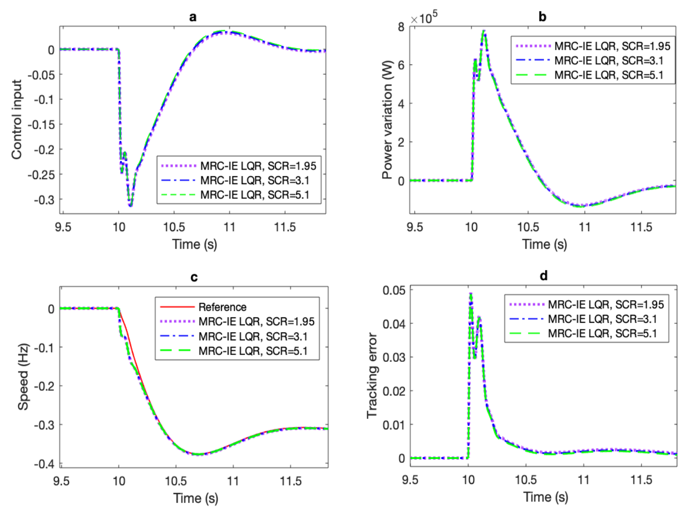

Fig. 10. Closed-loop performance under MRC based IE with LQR realization for different SCRs. (a) Control input. (b) Active power variation of WTG. (c) Speed of DSG. (d) Tracking error.

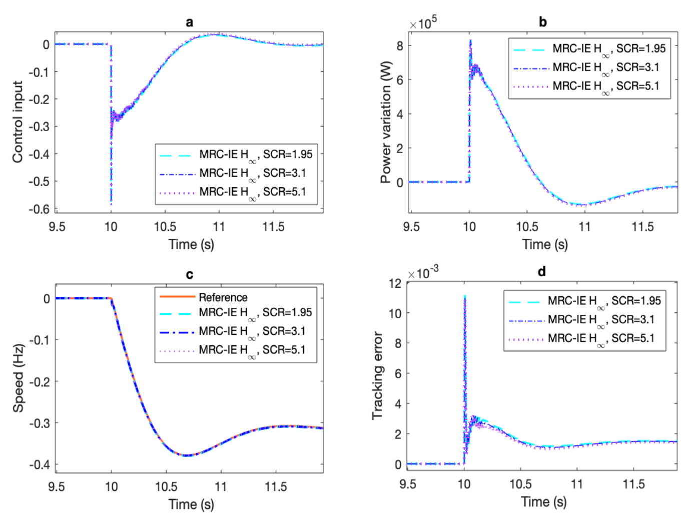

Fig. 11. Closed-loop performance under MRC based IE with H_∞ realization for different SCRs. (a) Control input. (b) Active power variation of WTG. (c) Speed of DSG. (d) Tracking error.

VI. Conclusions

In this paper, new output feedback LQR and H_∞ control laws for inertia emulation using balanced truncation and the Luenberger observer are proposed. The controllers are applied to the full order nonlinear model and compared favorably to a PI controller and a conventional inertia emulation using a washout filter. The diesel generator speed follows the reference model in the time scale of inertial response, and accurate emulated inertia is guaranteed by generating additional active power from the WTG. The performance of the closed loop system shows improved accuracy with the H_∞ controller relative to the LQR controller, although they both achieve the desired frequency response. Therefore, without providing a specified margin for the frequency, adequate frequency response with robustness in the presence of disturbances can be achieved by setting the desired inertia based on the network operating point. The proposed technique is analyzed for different SCR scenarios where a lower bound to guarantee the performance is obtained.

Appendix A

Variables are in per unit unless specified otherwise. $S_{base} =$ 1.1 MVA, $V_{base} = 575$ V, $\bar{f} = 377$ (rad⁄s).

Operating condition: Wind speed: 11 m/s, $P_g = 0.8$, $Q_g = 0$, $V_{ds} = 0$, $V_{qs} = 1$.

Equilibrium point for the linearization: (for the dynamic equations) $\lambda_{ds} = 1.015$, $\lambda_{qs} = 0.002$, $\lambda_{dr} = 1.041$, $\lambda_{qr} = 0.223$, $\omega_r = 1.19$, $x_1 = -0.641$, $x_2 = 0.261$, $x_3 = 0.011$, $x_4 = 0.005$.

(For the algebraic equations) $i_{ds} = 0.084$, $i_{qs} = -0.631$, $i_{dr} = 0.261$, $i_{qr} = 0.671$, $V_{qr} = -0.196$, $V_{dr} = 0.048$.

Diesel generator: rated power $= 1$ MW, $H_D = 1$ (s), $\tau_{sm} = 0.1$ (s), $\tau_d = 0.2$ (s).

Wind turbine generator: rated power $= 1$ MW, $H_w = 2$ (s), $\tau_{sm} = 0.1$ (s), $\tau_d = 0.2$ (s), $K_{I_\tau} = 0.1$, $K_{P_c} = 0.6$, $K_{I_c} = 8$, $K_{I_Q} = 5$, $K_{P_Q} = 1$.

References

[1] Y. Zhang *et al.*, "Provision for guaranteed inertial response in diesel-wind systems via model reference control," *IEEE Trans. Power Syst.*, vol. 33, no. 6, pp. 6557–6568, 2018.

[2] M. Krpan and I. Kuzle, "Dynamic characteristics of virtual inertial response provision by DFIG-based wind turbines," *Electric Power Systems Research*, vol. 178, p. 106005, 2020.

[3] M. Krpan and I. Kuzle, "Coordinated control of an ultracapacitor bank and a variable-speed wind turbine generator for inertial response provision during low and above rated wind speeds," in *2019 IEEE Sustainable Power and Energy Conference (iSPEC)*, 2019, pp. 1693–1698.

[4] C. Wang, J. Li, and Y. Hu, "Frequency control of isolated wind-diesel microgrid power system by double equivalent-input-disturbance controllers," *IEEE Access*, vol. 7, pp. 105 617–105 626, 2019.

[5] S. Wang and K. Tomsovic, "A novel active power control framework for wind turbine generators to improve frequency response," *IEEE Trans. Power Syst.*, vol. 33, no. 6, pp. 6579–6589, 2018.

[6] M. Dreidy, H. Mokhlis, and S. Mekhilef, "Inertia response and frequency control techniques for renewable energy sources: A review," *Renewable and Sustainable Energy Reviews*, vol. 69, pp. 144–155, 2017.

[7] S. Morovati and H. Pulgar-Painemal, "Control coordination between dfig-based wind turbines and synchronous generators for optimal primary frequency response," *arXiv preprint arXiv:2009.07890*, 2020.

[8] H. J. Tessaro and R. V. de Oliveira, "Operating point optimization of wind turbine generators for provision of inertial response and frequency control," *International Transactions on Electrical Energy Systems*, vol. 30, no. 6, p. e12382, 2020.

[9] Z. Zhao *et al.*, "Multiple-time-scales hierarchical frequency stability control strategy of medium-voltage isolated microgrid," *IEEE Trans. on Power Electronics*, vol. 31, no. 8, pp. 5974–5991, 2016.

[10] J. Morren, S. W. H. de Haan, W. L. Kling, and J. A. Ferreira, "Wind turbines emulating inertia and supporting primary frequency control," *IEEE Trans. Power Syst.*, vol. 21, no. 1, pp. 433–434, 2006.

[11] M. Kayikci and J. V. Milanovic, "Dynamic contribution of dfig-based wind plants to system frequency disturbances," *IEEE Trans. Power Syst.*, vol. 24, no. 2, pp. 859–867, 2009.

[12] B. Wang, Y. Zhang, K. Sun, and K. Tomsovic, "Quantifying the synthetic inertia and load-damping effect of a converter-interfaced power source," in *2018 IEEE International Energy Conference (ENERGYCON)*, 2018, pp. 1–6.

[13] Y. Zhang, K. Tomsovic, S. M. Djouadi, and H. Pulgar-Painemal, "Hybrid controller for wind turbine generators to ensure adequate frequency response in power networks," *IEEE J. Emerg. Sel. Topics Circuits Syst.*, vol. 7, no. 3, pp. 359–370, 2017.

[14] S. D'Arco and J. A. Suul, "Equivalence of virtual synchronous machines and frequency-droops for converter-based microgrids," *IEEE Trans. on Smart Grid*, vol. 5, no. 1, pp. 394–395, 2014.

[15] Y. Zhang, A. Melin, S. Djouadi, and M. Olama, "Performance guaranteed inertia emulation for diesel-wind system feed microgrid via model reference control," in *2017 IEEE Power Energy Society Innovative Smart Grid Technologies Conference (ISGT)*, 2017, pp. 1–5.

[16] M. Krpan and I. Kuzle, "Introducing low-order system frequency response modelling of a future power system with high penetration of wind power plants with frequency support capabilities," *IET Renewable Power Generation*, vol. 12, no. 13, pp. 1453–1461, 2018.

[17] J. G. Slootweg, S. W. H. de Haan, H. Polinder, and W. L. Kling, "General model for representing variable speed wind turbines in power system dynamics simulations," *IEEE Trans. Power Syst.*, vol. 18, no. 1, pp. 144–151, 2003.

[18] G. S. Kaloi, J. Wang, and M. H. Baloch, "Active and reactive power control of the doubly fed induction generator based on wind energy conversion system," *Energy Reports*, vol. 2, pp. 194–200, 2016.

[19] N. R. Ullah, T. Thiringer, and D. Karlsson, "Temporary primary frequency control support by variable speed wind turbines— potential and applications," vol. 23, no. 2, pp. 601–612, 2008.

[20] H. A. Pulgar-Painemal, "Wind farm model for power system stability analysis," Ph.D. dissertation, Univ. of Illinois at Urbana-Champaign, Champaign, IL, 2010.

[21] S. Sahyoun, J. Dong, and S. M. Djouadi, "Reduced order modeling for fluid flows based on nonlinear balanced truncation," in *2013 American Control Conference*, 2013, pp. 1284–1289.

[22] A. C. Antoulas, D. C. Sorensen, and S. Gugercin, "A survey of model reduction methods for large-scale systems," *Contemporary Mathematics*, vol. 280, pp. 193–219, 2001.

[23] B. Moore, "Principal component analysis in linear systems: Controllability, observability, and model reduction," *IEEE Trans. on Automatic Control*, vol. 26, no. 1, pp. 17–32, 1981.

[24] K. Willcox and J. Peraire, "Balanced Model Reduction via the Proper Orthogonal Decomposition," *AIAA Journal*, vol. 40, no. 11, pp. 2323–2330, 2002.

[25] R. C. Camphouse, S. M. Djouadi, and J. H. Myatt, "Feedback control for aerodynamics (preprint)," 2006.

[26] K. Zhou and J. C. Doyle, "Essentials of robust control," 1997.

[27] M. E. Baran and F. F. Wu, "Network reconfiguration in distribution systems for loss reduction and load balancing," *IEEE Power Engineering Review*, vol. 9, no. 4, pp. 101–102, 1989.

[28] P. W. Sauer and M. Pai, *Power system dynamics and stability*. New Jersey, USA: Prentice Hall, 1997.

[29] N. Nimpitiwan, G. T. Heydt, R. Ayyanar, and S. Suryanarayanan, "Fault current contribution from synchronous machine and inverter based distributed generators," *IEEE Transactions on Power Delivery*, vol. 22, no. 1, pp. 634–641, 2007.

[30] J. W. Feltes and B. Fernandes, "Wind turbine generator dynamic performance with weak transmission grids," in *2012 IEEE Power and Energy Society General Meeting*. IEEE, 2012, pp. 1–7.

[31] J. O. Tande, G. Di Marzio, and K. Uhlen, "System requirements for wind power plants," *SINTEF energy res*, 2007.

[32] J. Ahnlund, "Short-circuit contributions from fully-rated converter wind turbines: Modeling and simulation of steady-state short-circuit contributions from frc wind turbines in offshore wind power plants," 2014.

[33] Y. Zhang *et al.*, "Evaluating system strength for large-scale wind plant integration," in *2014 IEEE PES General Meeting — Conference Exposition*, 2014, pp. 1–5.

Samaneh Morovati (GS'16) received the B.S. degree in Electrical Engineering with a concentration in control systems from Imam Khomeini International University, Iran, in 2011 and the M.S. degree in Electrical Engineering with a concentration in control and signalling from Iran University of Science and Technology, Iran, in 2017. She is currently pursuing the Ph.D. in Electrical Engineering at the University of Tennessee, Knoxville, TN, USA. Her main research interests include control system theory, distributed and decentralized control, power system dynamics, renewable energy and smart grids.

Yichen Zhang (S'13–M'18) received the B.S. degree in electrical engineering from Northwestern Polytechnical University, Xi'an, China, in 2010, the M.S. degree in electrical engineering from Xi'an Jiaotong University, Xi'an, China, in 2012, and the Ph.D. degree in electrical engineering from the Department of Electrical Engineering and Computer Science, University of Tennessee, Knoxville, TN, USA, in 2018. He was also a research assistant with the Oak Ridge National Laboratory from 2016-2018. He is currently a post-doctoral appointee with the Energy Systems Division, Argonne National Laboratory. His research interests include power system dynamics, grid-interactive converters, control and decision-making for cyber-physical power systems.

Seddik M. Djouadi (M'99-SM'20) received the Ph.D. degree from McGill University, the M.Sc. degree from University of Montreal, both in Montreal, the B.S. (with first class honors) from Ecole Nationale Polytechnique, Algiers, El Harrach, Algeria, all in electrical engineering in 1999, 1992, and 1989, respectively. He is currently a Full Professor in the Electrical Engineering and Computer Science Department, University of Tennessee, Knoxville. Prior to joining the University of Tennessee, he was an Assistant Professor in the University of Arkansas at Little Rock, and held postdoctoral positions in the Air Force Research Laboratory and Georgia Institute of Technology, where he was also a Design Engineer with American Flywheel Systems Inc.

His research interests include filtering and control of systems under communication constraints, modeling and control of wireless networks, control systems and applications to autonomous sensor platforms, electromechanical and mo- bile communication systems, in particular smart grid and power systems, control systems through communication links, networked control systems, and model reduction for aerodynamic feedback flow control.

Dr. Djouadi received five US Air Force Summer Faculty Fellowships, and five Oak Ridge National Laboratory Summer Fellowships. He received the Best Paper Award in the 1st Conference on Intelligent Systems and Automation 2008, the Ralph E. Powe Junior Faculty Enhancement Award in 2005, the Tib- bet Award with AFS, Inc., in 1999, and the American Control Conference Best Student Paper Certificate (best five in competition) in 1998. He was selected by Automatica twice as an outstanding reviewer for 2002–2003 and 2003–2004.

Kevin Tomsovic (F'07) received the BS from Michigan Tech. University, Houghton, in 1982, and the MS and Ph.D. degrees from University of Washington, Seattle, in 1984 and 1987, respectively, all in Electrical Engineering. He is currently the CTI Professor with the Department of Electrical Engineering and Computer Science, University of Tennessee, Knoxville, TN, USA, where he also directs the NSF/DOE ERC, the Center for Ultra-Wide-Area Resilient Electric Energy Transmission Networks (CURENT), and has also served as the Electrical Engineering and Computer Science Department Head from 2008 to 2013. He was on the faculty of Washington State University, Pullman, WA, USA, from 1992 to 2008. He held the Advanced Technology for Electrical Energy Chair with Kumamoto University, Kumamoto, Japan, from 1999 to 2000, and was the NSF Program Director with the Electrical and Communications Systems Division of the Engineering Directorate from 2004 to 2006. He has also held positions at National Cheng Kung University and National Sun Yat Sen University in Taiwan from 1988-1991 and the Royal Instituted of Technology in Sweden from 1991-1992. He is a Fellow of the IEEE.

Andrew Wintenberg (GS'20) was born in Knoxville, Tennessee, USA, in 1996. He received his B.S. degree in Electrical Engineering and Mathematics from The University of Tennessee, Knoxville, USA, in 2018 and his M.S. degree in Electrical Engineering from the University of Michigan, Ann Arbor, in 2020, where he is currently a Ph.D candidate. His research interests include the safety and security of discrete-event and cyber-physical systems through formal methods and abstraction.

Mohammed Olama (S'98-M'08-SM'19) received the B.S. and M.S. (Hons.) degrees in electrical engineering from the University of Jordan, Amman, Jordan, in 1998 and 2001, respectively, and the Ph.D. degree from the University of Tennessee, Knoxville, TN, USA, in 2007. He is currently a Senior Research Scientist with the Computational Sciences and Engineering Division, Oak Ridge National Laboratory, Oak Ridge, TN, USA. He is also an Adjunct Associate Professor with the EECS Department at the University of Tennessee, Knoxville, TN, USA. He has more than 160 archival publications (including journals, conference proceedings, book chapters, and technical reports) in addition to numerous presentations at professional conferences and international symposia. His research interests include smart grid and smart buildings; smart grid communications and control; building-to-grid integration; cyber-physical systems; complex systems; wireless communications; healthcare data analytics; machine learning; artificial intelligence; statistical signal processing; and discrete-event simulation.